River Surface Analysis and Characterization Using FMCW Radar

Marc A. Mutschler, *Student Member, IEEE*, Philipp A. Scharf, *Graduate Student Member, IEEE*, Patrick Rippl, *Graduate Student Member, IEEE*, Timo Gessler, Thomas Walter, *Member, IEEE*, and Christian Waldschmidt, *Fellow, IEEE*

***Abstract*—Today's warning systems for floods or droughts require sensor applications that provide a vast array of information. Current systems provide insight into either the water level or the river velocity. In order to obtain additional parameters for the characterization of the flow behavior in a noncontact manner, a frequency-modulated continuous-wave radar with chirp sequence is used. Since these sensors provide range and velocity information but also enable gathering of additional parameters. The presented measurements in this contribution were performed at four different rivers with a commercially available radar sensor. The results of the classical postprocessed 2-D fast Fourier transform are used as basis for an imagewise processing approach to obtain additional features for classifying the behavior of the river surface. For this purpose, the framewise enveloping velocities are depicted in a time sequence. Due to processing the detected reflection patterns in relation to time, a characteristic pattern for river flow profiles can be extracted. By reducing the information using time averaging, characteristic features for different flows can be extracted from the spatial envelope velocity distribution. In particular, the resulting insights lead to characteristic features for single flow distributions that enable novel monitoring systems with new possibilities to classify rivers using radar sensors.**

***Index Terms*—Characterization, chirp sequence radar, frequency-modulated continuous-wave (FMCW) radar, radar measurements, river hydraulics, surface velocity radars (SVRs).**

I. Introduction

CONTACTLESS measurements offer a significant advantage over sensor systems, which are in direct contact with the medium to be measured, especially in harsh environments, because the maintenance as well as the installation effort are reduced. It is evident that earlier intervention is realizable if warning systems detect a potential flood as early as possible [1]. Contactless radar-measuring systems have an advantage over the previously proven systems, such as purely mechanical systems (e.g., propeller current meter [2], [3]) or the frequently used ultrasonic measuring systems (see, e.g., [4], [5]), which are always in contact with the measured medium. Radar systems in particular can be used as an important supplement for flood early warning systems, as they can quickly and reliably provide information at critical points.

One of the most important parameters for monitoring natural river flows as well as artificially created channels is the volume flow rate, which is also called discharge. However, it is not possible to directly measure this parameter with sensors. Based on a detailed insight into the river bathymetry, water level height and water level velocity, it is possible to calculate the river discharge. While the bathymetry is roughly given for artificially created channels, it has to be estimated for natural riverbeds. There are various approaches to this, which are discussed in [5] and [6].

Radar sensors are able to directly measure the water surface level as well as the river surface velocity. Nowadays, a Doppler radar, which has also become established in a wide range of applications, is used for water surface velocity detection. The scope of activities range from flow measurements [7] to river flow monitoring [8], river profiling [9] in the UHF frequency range and up to 24 GHz [10] or 77 GHz systems [11], [12] detecting water surface velocities as well as water surface level determination [13]. Due to the complex hydrological mechanisms of natural rivers, the velocity distribution of the river cross section consists of a variety of velocities [14]. The velocities vary from zero at the riverbed to the maximum velocity just below the water surface [15]. Using appropriate modeling on the basis of entropy models [16], the mean velocity can be estimated as a function of the maximum occurring velocity [17]. This approach has also been successfully tested in [18] with a 24 GHz Doppler radar.

Regarding a flood warning system, the frequency-modulated continuous-wave (FMCW) radar offers the advantage of detecting the water surface level in addition to the surface velocity [19] compared with a Doppler radar. For a stationary mounted FMCW radar sensor, the obtained distance information indicates the surface level of the river taking into account the observation geometry. In this article, the use of commercially available FMCW radar sensors for river monitoring in real

Manuscript received October 11, 2021; revised December 8, 2021, January 19, 2022, and February 14, 2022; accepted February 25, 2022. Date of publication March 8, 2022; date of current version April 4, 2022. This work was supported in part by the European Regional Development Fund (ERDF) and in part by the Baden-Württemberg Ministry of Science, Research and Culture, through the project ZAFH MikroSens, in part by the Baden-Württemberg Ministry of Science, Research and Culture, and in part by the Ulm University of Applied Sciences through the funding programme Open Access Publishing. *(Corresponding author: Marc A. Mutschler.)*

Marc A. Mutschler and Patrick Rippl are with the Laboratory of Microtechnology, Ulm University of Applied Sciences, 89081 Ulm, Germany, and also with the Institute of Microwave, University of Ulm, 89081 Ulm, Germany (e-mail: marc.mutschler@thu.de; patrick.rippl@thu.de).

Philipp A. Scharf, Timo Gessler, and Thomas Walter are with the Laboratory of Microtechnology, Ulm University of Applied Sciences, 89081 Ulm, Germany (e-mail: philipp.scharf@thu.de; timo.gessler@thu.de; thomas.walter@thu.de).

Christian Waldschmidt is with the Institute of Microwave, University of Ulm, 89081 Ulm, Germany (e-mail: christian.waldschmidt@uni-ulm.de).

Digital Object Identifier 10.1109/JSTARS.2022.3157469

This work is licensed under a Creative Commons Attribution 4.0 License. For more information, see https://creativecommons.org/licenses/by/4.0/

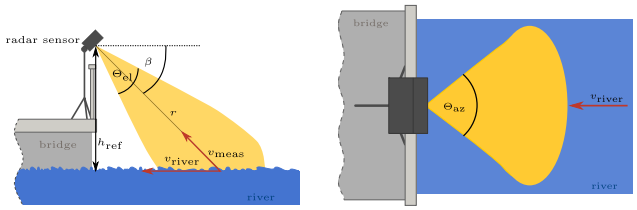

Fig. 1. Principle sketch of the measurement setup from (a) side and (b) top view to measure the river surface under an angle of view β with a radar sensor installed on a bridge. The observation area depends on the sensor height h and the beamwidth in elevation Θ_{el} and azimuth Θ_{az}.

environments will be shown. The main objective is to use FMCW measurements to determine characteristic features that contribute further parameters to classify the properties of the water surface in addition to the simple measurement of surface velocity and distance. Beside the classical hydrological parameters, these features show potential to improve flood warning systems. Special attention is paid to the information benefit resulting from the time series of the FMCW data regarding the temporal change of the water surface.

II. Methodology

Basically, the river surface is illuminated by a radar sensor to measure the electromagnetic wave backscattered by the rough water surface. Therefore, the radar sensor is installed on a bridge observing the flow of the river under a certain down-looking angle, as shown in Fig. 1. The reflection of electromagnetic waves from ocean or river waves is often attributed to the phenomenon of Bragg scattering [20], [21]. However, this theory requires a very specific situation-dependent relationship between the electromagnetic wave and a periodic surface structure. As shown in [22], backscattering does not consist exclusively of Bragg scattering, it is rather a superposition of the Bragg scattering and other effects. In [23], Fresnel reflections and multipath as well as multibounce scattering are used as explanations for nonBragg backscattering. In [24], Fresnel–Kirchhoff diffraction was shown to be an applicable approximation to radar backscattering, depending on the surface roughness and the frequency used. Assuming that random (rough) surfaces have a corresponding statistically distributed complex interference pattern or backscatter, the more universal Fresnel approach is more suitable for rough water surfaces of rivers. On river surfaces, where periodic components can rather be neglected, the Fresnel approximation allows the consideration of backscatter from a more statistical point of view, as it is probably the dominant component of backscatter. In this article, these backscattering structures are described as reflection centers, which are both moving and varying in rivers depending on their flow characteristics. This issue is discussed in more detail in the following.

A. Signal Processing

In contrast to studies with conventional continuous wave Doppler sensors, where a narrow beam is recommended to capture the surface velocity (see [18] and [20]), a wider beam is

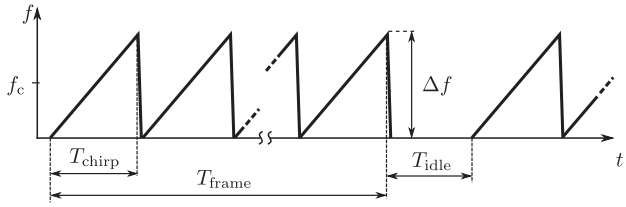

Fig. 2. Frequency ramps of a chirp-sequence FMCW transmit signal with highlighted frequency sweep Δf of the center frequency f_{c}, ramp time T_{ramp}, time for one frame T_{frame}, and the idle time T_{idle} between two successive frames.

used in this approach to capture further information of the water surface besides the surface velocity. The detected movement of the river, represented in the range-Doppler results of the chirped sequence FMCW sensor, is evaluated with regard to the distribution of the enveloping velocity. The results are enhanced by an integration gain due to a time averaging of a number of frames of the measurements. To obtain the range-Doppler results, the two-dimensional fast Fourier transform (2D-FFT) method with the typical intermediate frequency

$$f_{\text{IF}} = \underbrace{\frac{2\,\Delta f\,R}{c_0\,T_{\text{chirp}}}}_{f_{\text{r}}} + \underbrace{\frac{2\,f_{\text{c}}\,v_{\text{meas}}}{c_0}}_{f_{\text{d}}} \tag{1}$$

is processed, where Δf is the ramp bandwidth, R is the range, T_{chirp} is ramp duration, f_{r} is the range frequency, f_{c} is the center frequency, v_{meas} is the Doppler velocity measured by the radar sensor, c_0 is the speed of light in vacuum, and f_{d} is the Doppler frequency. The principle waveform of the transmitted chirp sequence signal is shown in Fig. 2. The 2D-FFT is performed using two successive fast Fourier transform (FFT) series. In the first step of the 2D-FFT, for each frame consisting of N chirps and a length of T_{frame}, a distance proportional FFT is calculated over each chirp of length T_{chirp} to extract f_{r}, as defined in (1). In the second dimension, subsequently FFTs are computed for each of the corresponding range cells (respectively, range FFT bins) to extract the velocity proportional parts f_d from (1). Since a radar can only detect radial velocities, the river surface velocity v_{river} can be calculated from the geometrical relation

$$v_{\text{river}} = \frac{v_{\text{meas}}}{\cos\beta} \tag{2}$$

with the angle of view β and the radial Doppler velocity v_{meas} detected by the radar sensor. For the results presented in this article, all velocity values are converted using this ratio with a constant $\beta = 45°$ of the line of sight component. This conversion will be discussed further in Section IV. The well-known 2D-FFT signal processing of one data frame leads to the depiction in a range-Doppler map and represents a snapshot in the time span T_{frame} of the radar field of view. As a result, a range-dependent velocity distribution can now be visualized for each frame in this 2-D range-Doppler map. In the following, a special focus is set on the envelope velocity distribution $v_{\text{env}}(r)$ as a function over range r to be used as a measure for the characterization of a river. Since the flow velocity of a river is significantly slower than one radar frame, the time average of multiple frames is taken into account for the evaluation in the approach presented

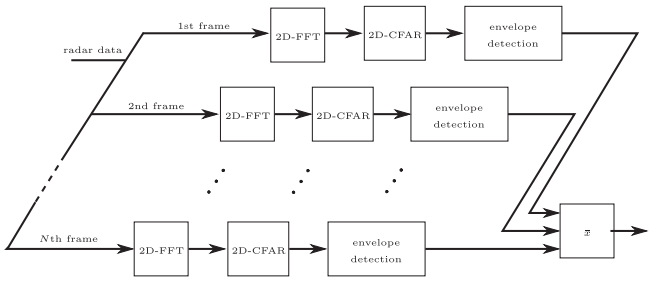

Fig. 3. Principle sketch of the signal processing.

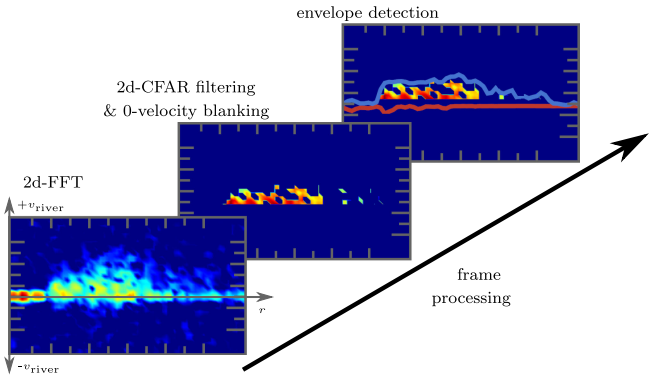

Fig. 4. Principle signal processing sketch of a single radar data frame.

in this article. In Fig. 3, the scheme of the radar data signal processing is illustrated.

To extract the envelope of the velocity distribution after the framewise 2D-FFT, a two-dimensional cell averaging constant false alarm rate (2D-CA-CFAR) filter is applied to the range-Doppler map of each frame. This processing step is to blank out the general noise environment around the actual water movements detected by the radar [25]. For this purpose, CA-CFAR calculates an averaged threshold around a series of test cells in the range-Doppler map depending on the signal amplitude of the surrounding cells (bins). The nearby cells around the test cell are excluded for the averaging. Only if the value of the test cell signal amplitude is above the calculated average threshold of the surrounding cells is it considered a target. Besides the CA-CFAR method, a modification of the CA or an ordered statistic CFAR could also be used, but these will not be examined further in this article. An overview of the different CFAR techniques can be found in [26], among others. In addition, a blanking of the zero Doppler line in the range of $\pm 0.1\ \mathrm{m/s}$ is performed. After these signal processing steps, the positive and negative envelope of the resulting detected velocity per range cell is calculated. By using an FMWC radar, it is possible to obtain positive and negative Doppler shifts within the range Doppler map after the 2-D FFT. In this article, velocities moving away from the radar are referred to as positive velocities and conversely, velocities moving toward the radar are referred to as negative velocities. The processing of a single frame dataset is given in Fig. 4 for an exemplary range-Doppler map.

Once the determination of the envelope velocity distribution over the distance $v_{\mathrm{env},k}$ for each frame $k \in [1, \ldots, N]$ of the N

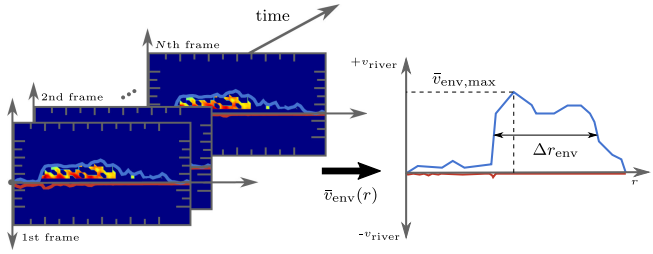

Fig. 5. Visualization of envelope velocity time averaging processing.

TABLE I
RADAR SENSOR AND WAVEFORM CONFIGURATION

f_c	Δf	T_{chirp}	T_{r}	Θ_{az}	Θ_{el}	f_{s}
77.5 GHz	3 GHz	100 µs	150 µs	28°	14°	10 MHz

frames is evaluated, a time averaged envelope velocity distribution

$$\bar{v}_{\mathrm{env}}(r) = \frac{1}{N} \sum_{k=1}^{N} v_{\mathrm{env},k}(r) \tag{3}$$

can be calculated for the entire data set, as shown in Fig. 5.

By averaging the envelope velocity distribution, on the one hand, a kind of integration gain is achieved, and on the other hand, a reduction of the information content is realized, which leads to a reliable statement about the characteristics of a river. As a measure for the characterization of a river, maximum velocity of the averaged envelope velocity distribution $\bar{v}_{\mathrm{env,max}}$ and the peak width Δr_{env} at $\frac{\bar{v}_{\mathrm{env,max}}}{2}$ of the envelope velocity profile is used in this approach. A visualization of these measures is also shown in Fig. 5. The example in Fig. 5 shows a prominent positive velocity distribution, representing a river flowing away from the radar.

B. Radar Sensor and Data Acquisition

For the measurements presented, a commercially available 76–81 GHz radar evaluation kit for industrial purpose [27] was utilized with a related analogue-to-digital converter module using a sampling frequency f_{s} of 10 MHz. The transmit and receive antennas are realized as microstrip patch antennas. In this article, only one receiving channel is used. In Table I, all important radar and waveform parameters of the used configuration related to Figs. 1 and 2 are summarized. The sidelobe levels of the radar in elevation are between a range of $\mathrm{SLL_{el}} = 10\ \mathrm{dB}$ at about 55° for 76 GHz $\mathrm{SLL_{el}} = 9.2\ \mathrm{dB}$ at about 42° for 78.5 GHz. Due to the mounting angle of the radar $\beta = 45°$, the first sidelobe in elevation is perpendicularly directed to the river surface. In azimuth, the sidelobe levels of the radar are between a range of $\mathrm{SLL_{az}} = 25\ \mathrm{dB}$ at about 165° for 76 GHz and $\mathrm{SLL_{az}} = 28\ \mathrm{dB}$ at about 161° for 78.5 GHz. The antenna diagrams can be found in the manufacturer's data sheet.

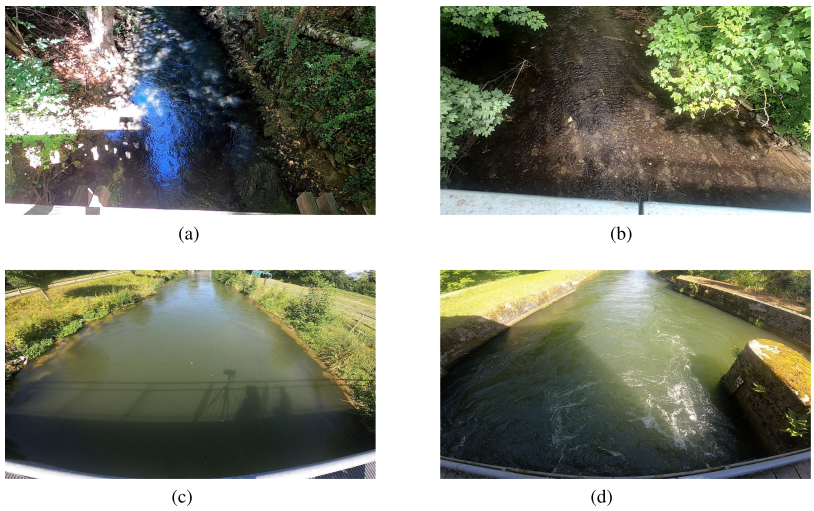

Fig. 6. Pictures of the four RUT. (a) River Blau with a small flow of water and a little turbulent water surface. (b) River Leibi with a fluctuating water surface and low water level. (c) Side channel of the river Iller with a high water level and smooth water flow. (d) Turbulent water discharge from a small hydroelectric power station on the Iller channel.

III. Results

In order to make a statement about the variation of the envelope peak width, four rivers in Southern Germany were analyzed. These rivers under test (RUTs) have different water surfaces and hydrological properties. In Fig. 6, photographs of the four RUTs are shown. In Fig. 6(a), the river Blau with a small flow of water and only few little turbulences on the water surface is shown. The river Leibi with a fluctuating water surface and low water level is shown in Fig. 6(b). In contrast, Fig. 6(c) shows a side channel of the river Iller with a high water level and smooth water flow. Finally, in Fig. 6(d), a turbulent water discharge from a small hydroelectric power station on the Iller channel is shown. The penetration depth of the radar at $77.5\,\mathrm{GHz}$ is very limited, so it can be assumed that the radar reflections are only affected by the water surface. In the following, the several intermediate results of the processing chain are described and explained.

A. 2D-FFT Results

The velocity distributions of the four RUTs after the initial 2D-FFT processing stage are shown in the range-Doppler maps (see Fig. 7). In Fig. 7, the abscissa shows the distance cells scaled to meters and the ordinate shows the Doppler velocity cells scaled to meters per second, as well as the normalized signal intensity in dB.

The range-Doppler maps illustrate the occurrences of reflection centers on the river surfaces. It is a momentary record of a certain time period. Using a set of 255 chirps per frame and the recovery time T_r given in Table I, the range-Doppler map represents a time period of $38.2\ \mathrm{ms}$. With the implemented waveform, it is possible to indicate velocities with a resolution of $\Delta v = v_\mathrm{meas,min} = \frac{c_0}{2 f_\mathrm{c} T_\mathrm{frame}} \approx 0.052\,\mathrm{m/s}$, whereby the frame duration T_frame is the influencing factor. The maximum detectable velocity $v_\mathrm{meas,max} = \frac{c_0}{4 f_\mathrm{c} T_\mathrm{r}} \approx 6.57\,\mathrm{m/s}$ is mainly influenced by the ramp recovery time T_r. Typically, the flow velocities of rivers are between 0.1 and $6\,\mathrm{m/s}$. Thus, the range-Doppler map of river, Fig. 7(a), does not contain high intensities. As expected for a slow flowing river, only low velocities are visible (approximately $-0.5\ \mathrm{m/s}$) and typical for a slow flowing river with a smooth surface, the range distribution is very limited. The negative sign here is due to the flow direction of the river, which in this case is in the direction of the radar. For the other RUTs, the flow direction is reversed and the sign is, therefore, positive.

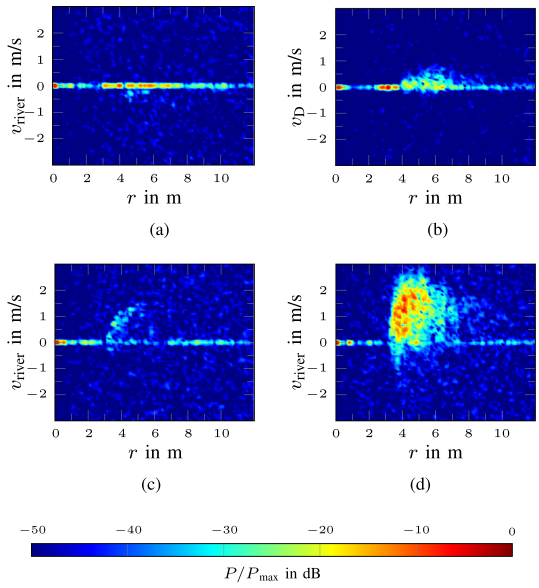

Fig. 7. Range-Doppler plots of a single frame for the four RUTs before zero velocity blanking and CFAR filtering post processing. (a) River Blau. (b) River Leibi. (c) Iller channel. (d) Hydroplant Iller.

As observable in Fig. 6(b), the corresponding range-Doppler map Fig. 7(b) of river (b) shows considerably more reflection centers. These reflection centers flow only slowly away from the radar (approximately $0.5\ \mathrm{m/s}$), but extend over about three meters.

In the range-Doppler map Fig. 7(c) of river (c), a typical J-hook like distribution of a water flow is recognizable up to about $1.4\ \mathrm{m/s}$. According to the smooth water flow pictured in

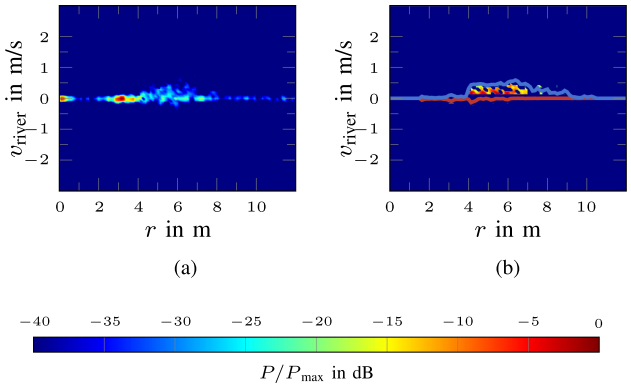

Fig. 8. Range-Doppler plot before and after postprocessing (2D-CFAR filtering and zero velocity blanking) exemplary for river Leibi [see Fig. 7(b)] with positive and negative envelope velocity distribution v_{env}. (a) Unfiltered 2D-FFT. (b) Filtered 2D-FFT with v_{env}.

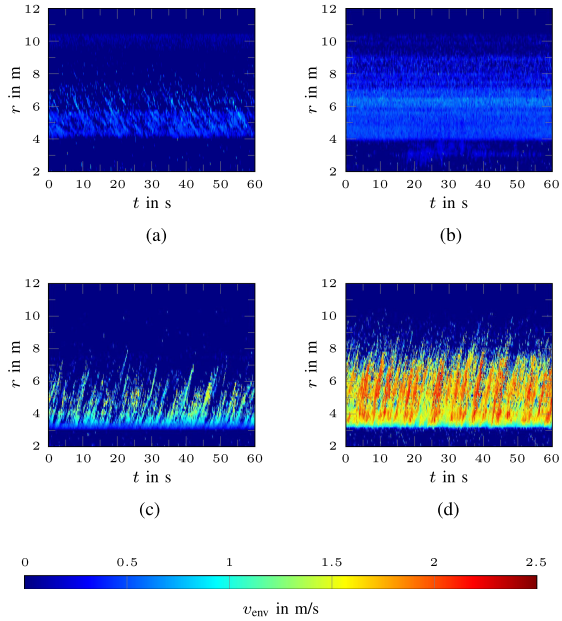

Fig. 9. Two dimensional time series plots of the absolute envelope velocity $v_{\text{env}}(t, r)$ in main flow direction over distance and time for each of the four RUTs. (a) River Blau. (b) River Leibi. (c) Iller channel. (d) Hydroplant Iller.

Fig. 6(b), the intensities are low and limited in range. The lack of sufficient reflection centers, due to gentle flow of water, leads to a low intensity, and thus also to a more localized detection of the water flow compared to the rough water surface at river (b) in Fig. 7(b) with a rougher river surface, and many reflection centers spread over several meters.

In the range-Doppler map of the river (d), a broad intensity distribution in both distance and velocity is clearly visible. As expected, river (d) contains the highest velocities compared to the other scenarios. As the river photography in Fig. 6(d) indicates the corresponding range-Doppler map [see Fig. 7(d)] shows a high amount of possible reflection centers, which are detectable over a broad distance range.

B. Zero Velocity Blanking and CFAR Filtering

In order to provide a more accurate indication about the characteristics of the river flow, and to reduce disturbances and noise, the zero velocity is blanked for the entire range-Doppler plots, and a 2D-CA-CFAR filter is used. Typically, a CFAR filter should be customized for each scenario. In the following, the same CFAR settings are used for all scenarios for better comparability. Fig. 8 presents the post-processed range-Doppler map of river flow (b) shown in Fig. 7(b). For a better understanding of the signal processing, Fig. 8(a) and (b) shows exemplary range-Doppler maps before and after CFAR filtering and zero velocity blanking as well as the envelope velocity distributions v_{env}, respectively. The envelope velocity is described in more detail in the following section. Due to the characteristics of the CFAR filter, after this processing stage, a statement of the exact maximum values in range or velocity is no longer possible, since intensity values below the threshold value are filtered out.

C. Envelope Velocity

Measurements with radar sensors are very fast compared with the flow velocity of rivers. Hence, to identify characteristics of reflection centers, a longer time interval of the flow must be observed. For this purpose, 600 consecutive radar frames or range-Doppler plots are evaluated, which covers a time period of $60\,\text{s}$. As a result, a snapshot measurement of the water is taken every $\frac{1}{10}$ of a second. In order to compare each of the frames with each other, the first step is to extract specific information of the range-Doppler plots. In the following, only the positive and negative velocities of the enveloping velocity profile per frame over range $v_{\text{env},k}(r)$ are used. As an exemplary representation, one postprocessed frame with highlighted positive and negative $v_{\text{env},k}(r)$ of river (b) is shown in Fig. 8(b). Placing these enveloping velocities in temporal sequence, one after the other, which corresponds to a framewise order, the resulting 2-D time series provides a statement concerning how the reflection centers of the flow evolve over time. These reflection centers of a RUT can originate partly from small flow waves or turbulences on the river surface. Fig. 9 shows the associated envelope velocities of the 2-D time series of the RUTs. In each case, the absolute velocities of the main flow directions are shown as intensities in range over time.

In Fig. 9(a), the pattern of weak reflection centers can be seen. It is noticeable that this river is flowing toward the sensor, and hence, the reflection centers are approaching the radar in temporal relation. Due to the nature of this smooth river surface, the detected reflections are rather weak and disappear within a short period of time. Between $4\,\text{m}$ and roughly $5.5\,\text{m}$, a nearly constant band of the radar main lobe reflection with about $0.5\,\text{m/s}$ is present.

In contrast to the abovementioned scenario, Fig. 9(b) shows a shallow flow. The fast fluctuating surface, which is flowing away from the sensor, leads to a reflection band between $4\,\text{m}$ and about $8\,\text{m}$ with a peak velocity of approximately $0.9\,\text{m/s}$. On this rapidly changing shallow water surface represented by the low intensity, no systematic time-depended reflection centers can be observed. The visible line of relatively low intensity at about $3\,\text{m}$ could be interpreted as branch movements of the

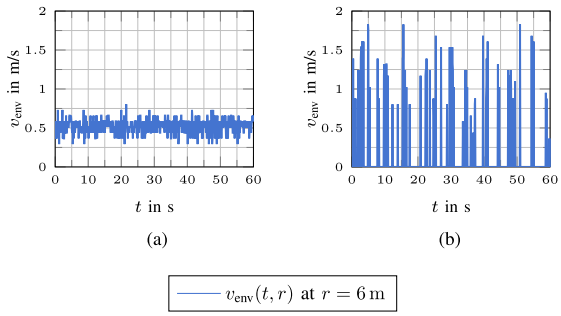

Fig. 10. Envelope velocity $v_{env}(t, r)$ cutout at 6 m of the two flows (a) Leibi and (b) Iller channel corresponding to the 2-D time series plots in Fig. 9(b) and (c).

surrounding trees, also visible in Fig. 6(b). This is supported by the distance of 3 m between the sensor and branches verified with a reference laser distance meter and the fact that the movement is not permanently noticeable in the time series plot. This point will be discussed in detail later.

While the photography [see Fig. 6(c)] depicts a very smooth water surface, the time series plot [see Fig. 9(c)] shows clear and persistent reflection centers flowing away from the sensor over time. These are visible from mainly 3.2 to 6 m and up to 7.5 m with a velocity up to 1.4 m/s.

In Fig. 9(d), an envelope velocity time series plot of the turbulent flow is shown. As it can be recognized in the photo [see Fig. 6(d)], significant, partially overlapping and frequently recurring reflection centers can be seen in the time series plot moving away from the radar sensor. The occurring reflection centers are clearly visible between 3.5 and 7 m up to almost 8 m. Velocities of up to 2.3 m/s were detected.

In this comparison, the differences between the flow in river (b) and the other rivers (a, c, and d) are particularly notable. To take a closer look at these differences, as shown in Fig. 10, a cut out at 6 m of the time series in Fig. 9 of river (b) and, representatively, of river (c) over time is shown. In Fig. 10(a), an almost constant envelope velocity cutout $v_{env}(t, 6\,\mathrm{m})$ at 6 m of river (b) at 0.6 m/s can be noticed and varies only slightly during the measurement time. In contrast, in Fig. 10(b), significant fluctuations of the envelope velocity of river (c) can be seen. The corresponding $v_{env}(t, 6\,\mathrm{m})$ of the reflection centers varies strongly over time. As a result, the individual values of $v_{env}(t, 6\,\mathrm{m})$ deviate strongly from the mean value. This is due to the fact that the detected reflection centers move over time. Here, in Fig. 10(b), only a section at 6 m is shown as an example, representing the change over time at this point. Compared with the other rivers, river (b) shows an almost constant local pattern of $v_{env}(t, r)$ over time at almost any distance, and the reflection centers do not move locally. In the case of the rivers (a), (c), and (d), the reflection centers do move spatially over time, which can be noticed in the 2-D time series plots depicted in Fig. 9 and results in the noncontinuous graph shown in Fig. 10(b), which exemplary shows river (c).

In order to create a quantitative measure for the characterization of the river flow features, the positive and negative

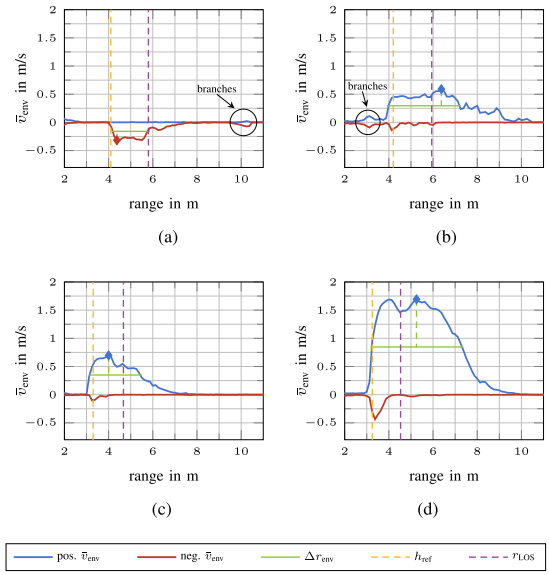

Fig. 11. Mean envelope velocity $\bar{v}_{env}$ (time averaged) over distance for each of the four RUT. Thereby, the positive part (—) and negative part (—) of the mean envelope velocities are depicted. The envelope velocity peak width in range Δr_{env} (—) maximum value $\bar{v}_{env,max}$ (marked with ♦) and the radar to water line of sight r_{LOS} (– –) as well as the reference height above the water surface h_{ref} (– –), which is measured with a laser range finder, are highlighted. (a) River Blau. (b) River Leibi. (c) Iller channel. (d) Hydroplant Iller.

mean envelope velocity are averaged over the time period of 60 s in the next processing step. The resulting mean envelope velocity distributions over range $\bar{v}_{env}(r)$ are shown in Fig. 11. In the respective figures of the RUTs, the features, such as the width as well as the maximum value (or respectively minimum, depending on the main flow direction) of the main flow velocity distribution, are highlighted. For an initial comparison of different RUTs, the values of the maximum mean velocity $\bar{v}_{env,max}$ and the mean envelope velocity peak width Δr_{env} at $\frac{\bar{v}_{env,max}}{2}$ are considered. The results are shown in Fig. 11.

As abovementioned, due to the mounting angle of the radar, the first elevation sidelobe perpendicularly illuminates the river surface. Hence, the radar does not detect any movement of the water smaller than the mounting height above the river surface. The marked reference height h_{ref} of the radar in Fig. 11 is measured with a laser rangefinder. The measurements from these laser rangefinders vary up to ±0.1 m relative to the actual water surface. Due to the physical property of water, the laser rangefinder cannot be applied to water surfaces, and therefore, reference points close to the river bank had to be chosen.

In Fig. 11(a), between 4.1 to 5.5 m, the mean envelope velocity $\bar{v}_{env}$ is approximately steady at −0.25 m/s with $\bar{v}_{env,max} = 0.3\,\mathrm{m/s}$ and $\Delta r_{env} = 1.54\,\mathrm{m}$. A quasi-symmetrical pattern of branch movements is noticeable at about 10.2 m. These can also be noticed in the measurements within the RUT analyzed in the following and will be discussed in more detail in a later section.

Fig. 11(b) shows a very fluctuating distribution of the $\bar{v}_{env}$, which starts at about 4 m and decreases slowly toward higher distances with $\bar{v}_{env,max} = 0.61\,\mathrm{m/s}$ at 6.4 m and $\Delta r_{env} = 3.09\,\mathrm{m}$. The peaks of positive and negative $\bar{v}_{env}$ at 3 m with a velocity of ±0.7 m/s are a distinctive characteristic of

this RUTs' fluctuating water surface. Remarkable is the peak with $-0.14\,\mathrm{m/s}$ at $4.13\,\mathrm{m}$. In this case, the peak does not reflect the velocity of the water surface, it is caused by the up and down movement of the water level directly under the sensor, which is detected by sidelobes in the range of the mounted sensors reference height h_{ref}. Similar patterns can be recognized in the measurements of the RUT analyzed in following. Especially at this RUT, where the water level is only a few centimeters, the water surface changes very quickly in vertical direction. Like in the previous RUT, a quasi-symmetrical pattern with a velocity of about $0.1\,\mathrm{m/s}$ is detected in this scenario at $3.1\,\mathrm{m}$, which also results from branch movements.

In Fig. 11(c), the mean envelope velocity begins at $3\,\mathrm{m}$, rapidly increasing to velocities about $0.6\,\mathrm{m/s}$ with $\bar{v}_{\mathrm{env,max}} = 0.68\,\mathrm{m/s}$. Thereafter, the velocity slowly decreases until it reaches $0\,\mathrm{m/s}$ at $7\,\mathrm{m}$, and leads to a Δr_{env} of $2.28\,\mathrm{m}$. A noticeable feature is the peak at $3.25\,\mathrm{m}$ with $-0.3\,\mathrm{m/s}$ of the negative $\bar{v}_{\mathrm{env}}$ curve. This matches the mounted height h_{ref} of the radar sensor directly above the water surface. As in Fig. 11(b), a positive range would also be visible, but this peak is superimposed by other reflections centers of the flow surface.

Fig. 11(d) shows the $\bar{v}_{\mathrm{env}}$ distribution of a turbulent flow with $\bar{v}_{\mathrm{env,max}} = 1.73\,\mathrm{m/s}$ and $\Delta r_{\mathrm{env}} = 4.64\,\mathrm{m}$. The positive velocity distribution ranges from about $3.1\,\mathrm{m}$ to almost $9\,\mathrm{m}$. The negative $\bar{v}_{\mathrm{env}}$ at $3.4\,\mathrm{m}$ with $-0.74\,\mathrm{m/s}$ represents, as in the previous figures, the up and down movements of direct sidelobe reflections corresponding to the height of the sensor above the river surface.

In addition to the water motions shown in the Fig. 11(a) and (b), movements of stationary surrounding influences can also be observed. In Fig. 11(a), small velocities in both positive and negative directions can be detected at about $10.2\,\mathrm{m}$ and in Fig. 11(b) at $3.1\,\mathrm{m}$. These indicate movements of branches caused by the surrounding environment. This will be discussed in more detail in Section III-E.

TABLE II
RESULTS OF ENVELOPE VELOCITY MEASURES

RUT	h_{ref} in m	$\bar{v}_{\mathrm{env,max}}$ in m/s	Δr_{env} in m
River Blau	4.1	-0.32	1.57
River Leibi	4.2	0.59	3.2
Iller channel	3.3	0.7	2.3
Iller hydro plant	3.2	1.69	4.08

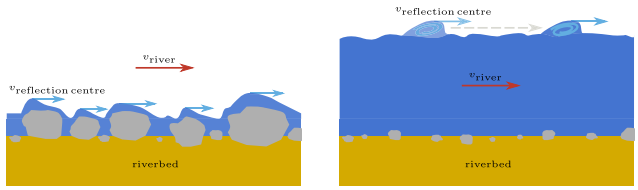

(a) (b)

Fig. 12. Principle riverbed illustration of a (a) shallow water level with spatially constant reflection centers (velocities detected by radar indicated with blue arrows) and (b) high water level river with moving reflection center (indicated by the gray dashed arrow).

TABLE III
MEAN VALUE AND STANDARD DEVIATION OF THE CHARACTERIZATION PARAMETERS AVERAGED OVER FIVE DIFFERENT MEASUREMENT SERIES

	$\bar{v}_{\mathrm{env}}$		Δr_{env}	
RUT	μ	σ	μ	σ
River Blau	-0.35	0.018	1.56	0.014
River Leibi	0.59	0.003	3.20	0.009
Iller channel	0.69	0.033	2.30	0.037
Iller hydro plant	1.71	0.025	4.13	0.053

D. Characterization of RUT

Especially the 2-D time series plots of the RUTs in Fig. 9 illustrate the reflection centers behavior of the river surface. With the introduced information reduction of range-Doppler series and the extraction of measures, such as maximal mean envelope velocity $\bar{v}_{\mathrm{env,max}}$ and mean envelope velocity peak width Δr_{env}, the shown river flows can be classified. It is also relevant to know the height at which the radar sensor was mounted above the RUT in order to indicate the illuminated area on the water surface. Besides the flow velocity, the water level has a significant influence on the surface illuminated by the radar. For shallow rivers, the influence of the riverbed on the water surface movements becomes more significant, thus, also affecting the reflection centers detected by the radar. In Table II, an overview of the measures $\bar{v}_{\mathrm{env,max}}$ and Δr_{env} as well as the reference height h_{ref} of the radar sensor above the RUT is shown. Besides the apparent characterization parameters of velocity, especially Δr_{env} provides a base for the characterization of the river surface. The gently flowing rivers (a) and (c) show a narrow Δr_{env} in contrast to the more turbulent flows (b) and (d). Both turbulent flows (b) and (d) differ, besides the maximum occurring velocities, mainly in the way the reflection centers emerge. The rather shallow flow of river (b) is mainly caused by the shallow water level and is primarily characterized by the water flowing over the river bed (e.g. stones) and results in locally stable reflection centers. In contrast, the reflection centers on the surfaces of river (d) are not shaped directly by the ground due to the higher water level. Furthermore, the results in Fig. 9(d) show indications of spatially moving reflection centers, which are the dominating part of the measured reflection centers. This is also the case for rivers (a) and (c). This relationship between the riverbeds and the differences of spatially constant and moving reflection centers is schematically depicted in Fig. 12. In order to analyze the significance and reproducibility as a measure of the efficiency of the parameters shown, five different series of measurements were carried out on each RUT. For the four rivers, the mean value μ as well as the standard deviation σ averaged over five measurement series of the characterization parameters maximum mean envelope velocity $\bar{v}_{\mathrm{env}}$ and envelope velocity peak width in range Δr_{env}, are given in Table III. The low standard deviation σ of the parameters $\bar{v}_{\mathrm{env}}$ and Δr_{env} indicates a certain reliability and repeatability.

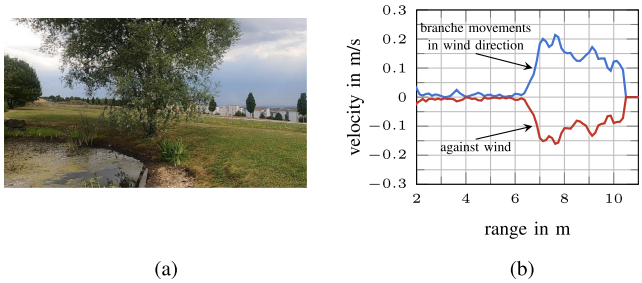

Fig. 13. Mean envelope velocity (averaged in time) over distance for a tree in a stationary environment. (a) Photography. (b) Envelope velocity.

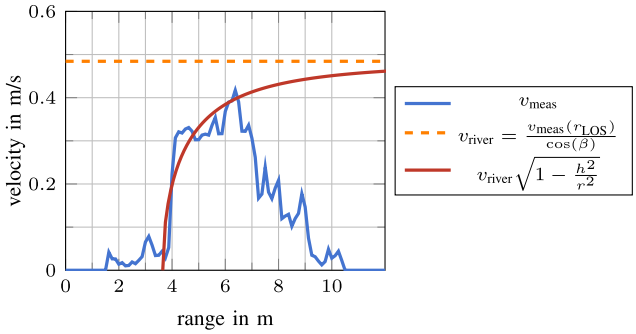

Fig. 14. Illustration of the measured uncorrected Doppler velocity v_{meas}, the interpreted v_{river} according the vector decomposition correction of (2) with $v_{\text{meas}}(r_{\text{LOS}})$ and the considered velocity distribution according (5) for the envelope velocity of the River Leibi according the measurements in Fig. 11(b).

E. Surrounding Influences

While the surroundings at the rivers (c) and (d) do not have significant influence on the resulting radar data, branches of trees and bushes can be seen at rivers (a) and (d) in the camera images [see Fig. 6(a) and (b)] and the resulting radar data. These can be separated by the spatial appearance or by the characteristics of the signals in the mean envelope velocity plot over range. A reference measurement of a tree moving in a moderate wind is shown in Fig. 13(b). The received signals are processed the same way as the river measurements shown before. The movement of the branches between 6.5 and $10.5\ \mathrm{m}$ with the wind creates a quasi-symmetrical movement in the mean envelope velocity plot in both the positive and negative velocity distributions over distance. A closer look reveals that the velocity amplitudes are not exactly symmetrical. The distribution in the direction of the wind is thereby more prominent ($0.2\ \mathrm{m/s}$) than in the direction against the wind ($-0.17\ \mathrm{m/s}$). One explanation for this characteristic could indicate that the velocity against the wind direction is lower than the movement in the wind direction due to the softer rebounding of the branches. Such characteristic branch movements can also be seen in the flow measurements Fig. 11(a) at $10.2\ \mathrm{m}$ and in Fig. 11(b) at $3.1\ \mathrm{m}$.

IV. Discussion

Compared with other studies that have already been undertaken on the topic of detecting the surface velocity of rivers (see [19] or [20]) or the mapping of the surface velocity to the actual river flow velocity (see[18]), this article has shown new opportunities for the use of FMCW radar sensors for river characterization. Especially, the evaluation of range-Doppler plots and the time-averaged velocity distribution of the envelope velocity distribution based on integration of several range-Doppler frames provide a deep insight. These evaluations contain a wide spectrum of information on the actual water surface that goes beyond the conventional consideration of water level and flow velocity. The extraction of these features was evaluated on four different rivers, which finally allow a characterization of these rivers. Specifically, the time sequence of the envelope velocity distribution over distance, including all frames allows a detailed analysis of the progression of the reflection centers at the river surface. Using this evaluation approach, a specific statement about the characteristics of the reflection centers detected by the radar can be made. In addition to the temporal course characteristics of reflection centers, temporal-stationary local reflection centers can also be distinguished and interpreted accordingly. In the method of plotting, a characterization of different types of rivers is possible, as these have different characteristics of the enveloping velocity distributed spatially and temporally. It was possible to identify characteristic branch movements in addition to the water movement. Through this characterization, branch movements can be separated from the water surface movement. The branch movement detection has also been proven in a second experiment. The river surface velocity results shown were adjusted as introduced in (2) with a constant factor of the vector decomposition for the line of sight component. For the purpose of characteristic extraction, this is an arguable approximation. For an accurate value of the actual surface velocity, this only matches for the velocity in the range $r = r_{\text{LOS}}$ of the line of sight component. Due to the radiation pattern of the radar, there are superpositions in the measured radial velocities in azimuth, and elevation of velocities occurring at the same distances at different radial angles. Based on the measurement setup, this superposition in elevation can be corrected by the separability in range. For this, the measured radial Doppler velocities have to be interpreted as a function of the range. Therefore, (2) has to be modified by the trigonometric relations

$$\sin\beta = \frac{h}{r} \tag{4}$$

and

$$\cos\beta = \sqrt{1-\sin^2\beta} \tag{5}$$

out of Fig. 1(a). With these relationships, the correlation

$$v_{\text{meas}} = v_{\text{river}}\sqrt{1-\frac{h^2}{r^2}} \tag{6}$$

between the measured radial velocity v_{meas} and the actual velocity of the river v_{river} depending on range r, sensor height h, and the corresponding angle β can be obtained. This correlation becomes problematic for values close to $r \approx h$. In Fig. 14, the illustration of the introduced equations for $r > h$ exemplary for the mean envelope velocity according Fig. 11(b) is shown. For the case $r \gg h$, the measured velocity approaches the actual

river velocity. However, this effect is unlikely to occur under real conditions, since for large r almost no radar backscatter can be expected. The measured uncorrected envelope velocity fits well into the considered velocity distribution. For this reason, a drop in the measured radial velocity can be seen after the LOS component at about $6\ \mathrm{m}$. Environmental factors, such as rain or wind, would affect the measurements of the surface velocity by influencing the structure of the river surface. The measurements presented in this article were performed in rainless and windless conditions, so the effects on the measurements could not be investigated. Another effect on the results are too smooth river surfaces where no water surface roughness is present. Most of the radar radiation will be reflected due to the dominating specular reflection. The rivers investigated in this article are not influenced by surface waves that can be caused by wind (see, e.g., [28]). However, in contrast to a conventional Doppler radar measurement, such surface waves could be interpreted separately from the flow velocity of the river through the representation in a 2-D time series. The same CFAR filter was used for postprocessing on the four different rivers, so there is still potential for improvement in the evaluation of the individual rivers through adaptation to the special scenarios.

Nevertheless, a long-term study on one and the same river would be very useful to consolidate the statements of this article and to categorize actual changes in the condition of the river surface in different scenarios, such as snow-melt, rain, or floods. The knowledge acquired in this way can then be used to improve flood warning systems or river monitoring.

V. Conclusion

The experiments in this article show the benefits that FMCW radar sensors can offer for river characterization and monitoring. On four rivers with significantly different characteristics, it was possible to show and compare several measures for the characterization of river flows with an FMCW radar. Besides the obvious features of detecting surface velocity and distance between water level and sensor, time-integrated features can provide more guidance to describe the characteristics of a river. The main objective is to investigate physically traceable parameters in a feature extraction that are feasible for averaged radar data. An essential task of feature extraction is the reduction of information, which is essential for large amounts of data. For this purpose, the approach of averaging several range-Doppler frames has been chosen as a central processing step. A detailed analysis of the time series plots of the envelope velocity curve integrated over each frame was performed to show the temporal progression of the reflection centers detected by the radar. These results can also be interesting for better understanding and optimizing common Doppler radar measurements on river surfaces. In addition, averaging the time series plots results in a characteristic velocity profile over range, which can be used for the characterization of river flows by the features maximum mean velocity and the width of the velocity profile. The resulting images of the reflection centers detected by the radar show interesting insights into the spatial and temporal changes and movements of these reflection centers. This provides an indication that the major component of radar backscattering on rivers is the more statistical interference-based Fresnel approach. Using these 2-D time series plots of the envelope velocities, a characterization of different river surfaces was realized as well as the detection of branch movements. By detecting the branch movement, these curves can be separated from the water movements. Especially the comparison of time varying parameters of the river surface offer significant additional insights, which provide more detailed information concerning the field of river monitoring and flood warning systems. An extended application of surface classification by radar systems to detect flotsam in order to identify blockages at an early stage is feasible.

References

[1] K. M. Carsell, N. D. Pingel, and D. T. Ford, "Quantifying the benefit of a flood warning system," *Nat. Hazards Rev.*, vol. 5, no. 3, pp. 131–140, Aug. 2004.

[2] A. Williams, "Current measurement technology development progress in the 90 s-A review," in *Proc. MTS/IEEE Conf. Coastal Ocean - Prospects 21st Century*, 1996, pp. 105–109.

[3] T. M. Hammond and M. B. Collins, "Flume studies of the response of various current meter rotor/ propellers to combinations of unidirectional and oscillary flow," *Deutsche Hydrografische Zeitschrift*, vol. 32, no. 2, pp. 39–58, 1979.

[4] K. Tezuka, M. Mori, T. Suzuki, and T. Kanamine, "Ultrasonic pulse-Doppler flow meter application for hydraulic power plants," *Flow Meas. Instrum.*, vol. 19, no. 3/4, pp. 155–162, Jun. 2008.

[5] M. Haide and W. Schroer, "Flow measurement in open channels by using an ultrasonic phased array sensor," in *Proc. IEEE Sensors*, 2013, pp. 1–4.

[6] T. Moramarco, S. Barbetta, D. M. Bjerklie, J. W. Fulton, and A. Tarpanelli, "River bathymetry estimate and discharge assessment from remote sensing," *Water Resour. Res.*, vol. 55, no. 8, pp. 6692–6711, Aug. 2019.

[7] Z. Ma, B. Wen, H. Zhou, C. Wang, and W. Yan, "UHF surface currents radar hardware system design," *IEEE Microw. Wireless Compon. Lett.*, vol. 15, no. 12, pp. 904–906, Dec. 2005.

[8] D. E. Barrick, C. C. Teague, and P. M. Lilleboe, "Systems and methods for monitoring river flow parameters using a VHF/UHF radar station," U.S. Patent No. 7,688,251, Mar. 30, 2010.

[9] D. Barrick, R. Cheng, C. Teague, J. Gartner, and P. Lilleboe, "Profiling river surface velocities and volume flow estimation with bistatic UHF riversonde radar," in *Proc. IEEE/OES 7th Work. Conf. Curr. Meas. Technol.*, 2003, pp. 55–59.

[10] Y. Lin, S. Chiu, and C. Chang, "A 24 GHz hydrology radar system capable of wide-range surface velocity detection for water resource management applications," *Microw. Opt. Technol. Lett.*, vol. 62, no. 11, pp. 3463–3475, Jun. 2020.

[11] C. Erhart, S. Lutz, J. Kohler, H. Mantz, T. Walter, and R. Weigel, "Surface velocity estimation of fluids using millimetre-wave radar," in *Proc. Eur. Microw. Conf.*, 2015, pp. 566–569.

[12] M. A. Mutschler *et al.*, "Time-domain correlation radar for fluid surface velocity estimation using a 77 GHz sensor platform," in *Proc. 14th Eur. Radar Conf.*, 2017, pp. 279–282.

[13] G. Wang, C. Gu, J. Rice, T. Inoue, and C. Li, "Highly accurate noncontact water level monitoring using continuous-wave Doppler radar," in *Proc. IEEE Topical Conf. Wireless Sensors Sensor Netw.*, 2013, pp. 19–21.

[14] R. Cheng and J. Gartner, "Complete velocity distribution in river cross-sections measured by acoustic instruments," in *Proc. IEEE/OES 7th Work. Conf. Curr. Meas. Technol.*, 2003, pp. 21–26.

[15] V. T. Chow, D. R. Maidment, and L. W. Mays, *Applied Hydrology (Letters)*. New York, NY, USA: McGraw-Hill, 1988.

[16] C. Chiu, "Entropy and 2-D velocity distribution in open channels," *J. Hydraulic Eng.*, vol. 114, no. 7, pp. 738–756, Jul. 1988.

[17] T. Moramarco, C. Saltalippi, and V. P. Singh, "Estimation of mean velocity in natural channels based on Chiu's velocity distribution equation," *J. Hydrologic Eng.*, vol. 9, no. 1, pp. 42–50, Jan. 2004.

[18] F. Alimenti *et al.*, "Noncontact measurement of river surface velocity and discharge estimation with a low-cost Doppler radar sensor," *IEEE Trans. Geosci. Remote Sens.*, vol. 58, no. 7, pp. 5195–5207, Jul. 2020.

[19] M. Scherhaufl, C. Hesch, and J.-M. Sevar, "Fluid surface velocity estimation using a 77 GHz radar module," in *Proc. IEEE Topical Conf. Wireless Sensors Sensor Netw.*, 2019, pp. 1–4.
[20] W. Plant, W. Keller, and K. Hayes, "Measurement of river surface currents with coherent microwave systems," *IEEE Trans. Geosci. Remote Sens.*, vol. 43, no. 6, pp. 1242–1257, Jun. 2005.
[21] W. J. Plant, "A model for microwave Doppler sea return at high incidence angles: Bragg scattering from bound, tilted waves," *J. Geophys. Res., Oceans*, vol. 102, no. C9, pp. 21131–21146, Sep. 1997.
[22] P. H. Lee *et al.*, "Experiments on Bragg and non-Bragg scattering using single-frequency and chirped radars," *Radio Sci.*, vol. 32, no. 5, pp. 1725–1744, Sep. 1997.
[23] P. H. Y. Lee *et al.*, "X band microwave backscattering from ocean waves," *J. Geophys. Res.: Oceans*, vol. 100, no. C2, pp. 2591–2611, Feb. 1995.
[24] P. A. Scharf, M. A. Mutschler, J. Iberle, H. Mantz, T. Walter, and C. Waldschmidt, "Spectroscopic estimation of surface roughness depth for mm-Wave radar sensors," in *Proc. 16th Eur. Radar Conf.*, 2019, pp. 93–96.
[25] B. R. Mahafza, *Radar Systems Analysis and Design Using MATLAB*. Boca Raton, FL, USA: Chapman & Hall/CRC, Apr. 2016.
[26] A. Jalil, H. Yousaf, and M. I. Baig, "Analysis of CFAR techniques," *Proc. 13th Int. Bhurban Conf. Appl. Sci. Technol.*, 2016, pp. 654–659.
[27] TI.com, "IWR1443BOOST IWR1443 single-chip 76-GHz to 81-GHz mmWave sensor evaluation module," Accessed: Nov. 11, 2021. [Online]. Available: https://www.ti.com/tool/IWR1443BOOST
[28] V. Gregers-Hansen and R. Mital, "An improved empirical model for radar sea clutter reflectivity," *IEEE Trans. Aerosp. Electron. Syst.*, vol. 48, no. 4, pp. 3512–3524, Oct. 2012.

Marc A. Mutschler (Student Member, IEEE) received the B.Eng. degree in mechatronics from the University of Applied Sciences Ulm, Ulm, Germany, in 2013, and the M.Sc. degree in electrical engineering from the University of Ulm, Ulm, Germany, in 2016. He is currently working toward the Dr.-Ing. degree in electrical engineering with the University of Applied Sciences Ulm in cooperation with the Department of Microwave Engineering, University of Ulm.

During this time, he has been researching information gathering from water surfaces using radar sensors. His research focuses on new approaches to the characterization and classification of water surfaces using mm-wave radar sensors.

Philipp A. Scharf (Graduate Student Member, IEEE) received the B.Eng. degree in mechatronics from the Ulm University of Applied Sciences, Ulm, Germany, in 2013, and the M.Eng. degree in electrical engineering from the Constance University of Applied Sciences, Constance, Germany, in 2015. He is currently working toward the Dr.-Ing. degree in electrical engineering with the Ulm University of Applied Sciences in cooperation with the Institute of Microwave Engineering, Ulm University, Ulm, Germany.

His research activities include multiband mmWave sensors and frequency-dependent scattering effects with focus on spectroscopic surface characterization.

Patrick Rippl (Graduate Student Member, IEEE) received the B.Sc. degree in mechatronics or robotics from the University of Applied Sciences Technikum Wien, Vienna, Austria, in 2014, and the M.Eng. degree in system engineering and management from the University of Applied Sciences Ulm, Ulm, Germany along with the M.Sc. degree in system engineering and management from the Rose Hulman Institute of Technology, Terre Haute, IN, USA in 2019. He is currently working toward the Dr.-Ing. degree in radar signal processing with the University of Applied Sciences Ulm in cooperation with the Department of Microwave Engineering, University of Ulm, Ulm, Germany.

His research interests include new approaches of classifying vulnerable road users and the simulation of traffic scenarios.

Timo Gessler received the B.Eng. degree in energy systems and the M.Eng. degree in electro mobility and electrical energy distribution from the University of Applied Sciences Ulm, Ulm, Germany, in 2015 and 2018, respectively.

He was a Research Assistant of radar research and target classification with the Laboratory for Microtechnology, University of Applied Sciences till 2020. He is currently a Test Engineer with automotive industry.

Thomas Walter (Member, IEEE) was born in 1963 in Sigmaringen, Germany. He received the Diploma in electrical engineering and the Ph.D. degree in research on electrical defects in thin film semiconductors from Stuttgart University, Stuttgart, Germany, in 1990 and 1995, respectively.

During this time, he studied for one year with the University of Northumbria, Newcastle, U.K. Then, he joined Robert Bosch, Stuttgart, Germany, working on microsystem technology, optical communication technology, and high-frequency electronics for automotive radars. During his R&D in industry, he was responsible for the introduction of SiGe-technology into 77 GHz radar sensors. In 2005, he joined the University of Applied Sciences Ulm as a Professor for microtechnology. He conducts several research projects on thin-film solar cells and microwave sensors. His research interests include microwaves and thin-film semiconductor.

Dr. Walter was the recipient of the Wissenschaftspreis der Stadt Ulm for his research on microwave sensors in 2012 and a scholarship from Studienstiftung des deutschen Volkes as a Student. He is a Reviewer of several IEEE and MDPI journals.

Christian Waldschmidt (Fellow, IEEE) received the Dipl.-Ing. (M.S.E.E.) and Dr.-Ing. (Ph.D.E.E.) degrees in electrical engineering from the University Karlsruhe, Karlsruhe, Germany, in 2001 and 2004, respectively.

From 2001 to 2004, he was a Research Assistant with the Institut für Höchstfrequenztechnik and Elektronik, Universität Karlsruhe. Since 2004, he has been with Robert Bosch GmbH, in the business units Corporate Research and Chassis Systems. He was heading different research and development teams in microwave engineering, RF-sensing, and automotive radar. In 2013, he returned to academia. He was appointed as the Director of the Institute of Microwave Engineering, University Ulm, Ulm, Germany, where he is a Full Professor. He has authored or coauthored more than 200 scientific papers and more than 20 patents. His research interests include radar and RF-sensing, mm-Wave and submillimeter-wave engineering, antennas and antenna arrays, RF, and array signal processing.

Dr. Waldschmidt is a Member of the Executive Committee Board of the German MTT/AP joint chapter and German Information Technology Society. He is currently the Chair of the IEEE MTT-29 Technical Committee on Microwave Aerospace Systems and was the Chair of MTT-27 Technical Committee on Wireless Enabled Automotive and Vehicular Applications. He was a two-time TPC Chair and the General Chair of the IEEE MTT International Conference on Microwaves for Intelligent Mobility. Since 2018, he has been an Associate Editor for IEEE MTT MICROWAVE WIRELESS COMPONENTS LETTERS. He is currently a Reviewer for multiple IEEE transactions and many IEEE conferences in the field of microwaves. Since 2014, he has been the co-recipient of 11 best paper awards.